Environmental Pollution 398 (2026) 128111

Contents lists available at ScienceDirect

Environmental Pollution

journal homepage: www.elsevier.com/locate/envpol

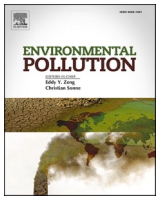

Uptake, metabolism, and transcriptome responses to 6PPD-Quinone in germinating *Ipomoea aquatica*

Shujia Wang [a,1], Linbin Zhu [b,1], Hua Yin [a,*], Minghan Zhu [a,b], Yuhao Cai [a], Chang He [c], Yuanyuan Yu [a,**], Shaoyu Tang [b]

[a] Key Laboratory of Ministry of Education on Pollution Control and Ecosystem Restoration in Industry Clusters, Guangdong Provincial Key Laboratory of Solid Wastes Pollution Control and Recycling, School of Environment and Energy, South China University of Technology, Guangzhou 510006, Guangdong, China
[b] School of Environment and Civil Engineering, Dongguan University of Technology, Dongguan, 523808, China
[c] Guangdong-Hong Kong-Macao Joint Laboratory for Contaminants Exposure and Health, Guangdong Key Laboratory of Environmental Catalysis and Health Risk Control, Institute of Environmental Health and Pollution control, Guangdong University of Technology, Guangzhou, 510006, China

ARTICLE INFO

Handling editor: Ying Guo

Keywords:
6PPD-Quinone
Uptake
Translocation
Transformation
Transcriptomics

ABSTRACT

N-(1,3-dimethylbutyl)-N′-phenyl-p-phenylenediamine-quinone (6PPD-Q), a transformation product of the widely used tire antioxidant 6PPD, has emerged as a ubiquitous environmental contaminant with potential risks to agroecosystems and food safety. This study systematically investigated 6PPD-Q uptake, translocation, transformation, and transcriptomic responses in the germinating leafy vegetable *Ipomoea aquatica*. In low, medium and high exposure groups, 6PPD-Q preferentially accumulated in roots, reaching concentrations of 17.8 ± 0.7, 55.3 ± 2.9 and 1414.5 ± 17.3 ng/g, respectively. High exposure to 6PPD-Q significantly inhibited seed germination and biomass accumulation, concomitant with the induction of oxidative stress. Nineteen 6PPD-Q transformation products were identified (*e.g.,* $C_{18}H_{22}N_2O_3$, $C_{22}H_{27}N_5O_9S$, $C_{24}H_{34}N_2O_7$, $C_{12}H_{20}N_2O$, and $C_7H_{13}NO_3$), revealing novel metabolic pathways including glycosylation, methoxylation, glutathionylation, oxidization, and carboxylation. Notably, several transformation products (*e.g.,* $C_{19}H_{24}N_2O_2$, $C_{18}H_{24}N_2O$) were predicted to be more toxic than the parent compound based on ECOSAR modeling, highlighting a potential secondary risk. Transcriptomic analysis suggested that the up-regulated genes encoding ABC transporters, cytochrome P450s, glutathione S-transferases, peroxidases, and UDP-glycosyltransferases likely played a role in the transmembrane transport and metabolic transformation of 6PPD-Q. Furthermore, the up-regulation of antioxidant genes and down-regulation of stress responsive genes indicated that 6PPD-Q exposure disrupted the balance between growth and stress defense. This study provides a comprehensive metabolic and molecular framework for understanding the fate of 6PPD-Q in an edible plant.

1. Introduction

The widespread use of synthetic antioxidants in vehicle tires has led to the environmental emergence of N-(1,3-dimethylbutyl)-N′-phenyl-p-phenylenediamine (6PPD), a chemical added to rubber formulations to prevent ozone-induced cracking (Rossomme et al., 2023). Upon environmental exposure, particularly through ozonation, 6PPD undergoes rapid transformation to form 6PPD-quinone (6PPD-Q), a highly toxic oxidation product (Hu et al., 2022). In recent years, 6PPD-Q has gained global attention as a contaminant of emerging concern due to its acute toxicity to aquatic ecosystems, notably causing mortality in coho salmon at ng/L levels (Tian et al., 2021, 2022). Moreover, 6PPD-Q can cause neurotoxicity (He et al., 2023), behavioral abnormalities (Hua et al., 2023), liver damage (Bohara et al., 2024; Liu et al., 2024), growth and

* Corresponding author. Key Laboratory of Ministry of Education on Pollution Control and Ecosystem Restoration in Industry Clusters, Guangdong Provincial Key Laboratory of Solid Wastes Pollution Control and Recycling, School of Environment and Energy, South China University of Technology, Guangzhou 510006, Guangdong, China.
** Corresponding author. Key Laboratory of Ministry of Education on Pollution Control and Ecosystem Restoration in Industry Clusters, Guangdong Provincial Key Laboratory of Solid Wastes Pollution Control and Recycling, School of Environment and Energy, South China University of Technology, Guangzhou 510006, Guangdong, China.
E-mail addresses: huayin@scut.edu.cn (H. Yin), 690480735@qq.com (Y. Yu).
[1] These authors contributed equally to this work.

https://doi.org/10.1016/j.envpol.2026.128111
Received 5 February 2026; Received in revised form 21 March 2026; Accepted 8 April 2026
Available online 12 April 2026

reproductive impairments (Shi et al., 2024), and oxidative stress (Sun et al., 2025). Many studies have reported the widespread detection of 6PPD-Q in various environmental matrices, including surface runoff (Tian et al., 2021; Wang et al., 2025a), road dust (Cao et al., 2022a), and soil (Hiki and Yamamoto, 2022). Soil contamination by 6PPD-Q largely results from tire wear particles (TWPs), which are deposited on road surfaces and subsequently washed into surrounding environments through stormwater runoff. Field investigations have reported the presence of 6PPD-Q in roadside soils at concentrations ranging from 9.5 to 936 ng/g (Cao et al., 2022a), and in industrial area soil at 0.002-4.4 ng/g (Zhang et al., 2024).

6PPD-Q ($C_{18}H_{24}N_2O_2$) has a molecular weight of 300.4. It is a lipophilic compound with a log K_{ow} of approximately 5.6, indicating high hydrophobicity (Castan et al., 2023). Consequently, it exhibits strong affinity for soil organic matter and tends to persist in the terrestrial environment. Plants are known to absorb a variety of environmental pollutants, including heavy metals (Deng et al., 2016; Seneviratne et al., 2019), pesticides (Xia et al., 2024), microplastics (Boots et al., 2019; Shi et al., 2022), and pharmaceutical residues (Tanoue et al., 2012), through root uptake from contaminated soils. Once taken up by plant roots, these chemicals may be translocated to aboveground tissues and undergo metabolic transformation. 6PPD-Q has been increasingly detected in environmental matrices and may also occur in agricultural fields near urban infrastructure. Therefore, it is critical to determine whether this contaminant can be taken up and transformed by edible plants, particularly during sensitive stages such as germination. A recent study demonstrated that 6PPD, at concentrations ranging from 10 to 400 μg/L, significantly inhibited the germination index, germination rate, vigor index, and shoot length of wheat (Baig et al., 2025). This highlights that germinating seedlings can serve as a critical model for investigating early uptake dynamics, antioxidant enzyme activities, and metabolic response (Baig et al., 2025). However, specific uptake, translocation, and antioxidant response of the more toxic derivative 6PPD-Q in edible vegetables during germination remain unknown. Moreover, the in planta transformation pathways of 6PPD-Q and ecological risks of its transformation products are still largely unexplored.

Recent advances in high-resolution mass spectrometry (Castan et al., 2023) and transcriptomic profiling (Yu et al., 2024b) have enabled detailed investigations into metabolic and molecular responses of plants to chemical pollutants. Plants possess complex enzymatic systems capable of transforming xenobiotics (Sun et al., 2018). These transformations can detoxify harmful compounds or produce intermediates with enhanced toxicity or persistence (Zhang et al., 2025b). Previous studies have shown that plants are capable of transforming various organic pollutants via phase I (hydrolysis, *etc.*) and phase II (conjugation, *etc.*) pathways (Kurade et al., 2019; Bauer et al., 2018). Thus, elucidating the *in vivo* metabolic fate of 6PPD-Q in plants is crucial for a comprehensive understanding of its ecological and health implications. In previous study, researchers have investigated 6PPD-Q in the soil nematode *Caenorhabditis elegans*, which clearly demonstrated the role of enzymes such as cytochrome P450 enzymes (CYP450s) and uridine diphosphate (UDP)-glycosyltransferases (UGTs) in 6PPD-Q degradation (Wang et al., 2025b). Moreover, research in lettuce (*Lactuca sativa*) has provided insights into 6PPD-Q uptake and transformation (Castan et al., 2023). Nevertheless, key aspects remain unresolved, including the complexity of 6PPD-Q transformation, toxicity of phase II metabolic intermediates, and underlying transformation mechanisms. To address these gaps, this study focuses on the sensitive germination stage and employs systematic in planta toxicity prediction for transformation products, integrated with transcriptomic analysis to elucidate molecular mechanisms.

In this study, we systematically investigated 6PPD-Q uptake, translocation, transformation, and transcriptomic responses in a typical leafy vegetable, *Ipomoea aquatica*, during germination. We aimed to (1) quantify 6PPD-Q accumulation in plants, (2) analyze antioxidant and physiological responses, (3) characterize metabolic transformation products, and (4) elucidate molecular mechanisms underlying plant defense and transformation. This study clarifies the environmental behavior of 6PPD-Q in plants, providing critical data for assessing its potential for food chain transfer and ecological risks in terrestrial environments.

2. Methods

2.1. Chemicals and materials

6PPD-Q (CAS: 2754428-18-5, 99.2%) was purchased from Shanghai Sayles Biochemical Technology Co., Ltd. For precise quantification, the corresponding stable isotope-labeled internal standard (^{13}C-labeled 6PPD-Q) was obtained from HPC Standards GmbH, Germany. All chemical reagents were acquired from Guangzhou Qianhui Chemical Glass Instrument Co., Ltd., including 30% hydrogen peroxide (H_2O_2) and HPLC-grade acetonitrile. Graphitized carbon black adsorbent was purchased from Ningbo Hongpu Experimental Technology Co., Ltd. Commercial fertilizer mixtures and *Ipomoea aquatica* seeds were procured from local markets. The experimental soil samples were collected from the South China University of Technology campus in Guangzhou, China (23.0547°N, 113.4011°E). The sampling site was a forested area approximately 5 m from a roadside near the university gate. Detailed soil sampling, preparation, extraction, and physicochemical properties are provided in Text S1.

2.2. Exposure experiments

The experimental design was based on the reported soil concentrations of 6PPD-Q, which ranged from 9.5 to 936 ng/g in roadside environments with a median of 234 ng/g (Cao et al., 2022a). We established three treatment groups for *Ipomoea aquatica*, including a low exposure group (group L, representing ambient background), a medium exposure group (group M, 200 ng/g) and a high exposure group (group H, 2000 ng/g). Measured initial soil concentrations were 33.2 ± 2.1, 185.8 ± 11.6, and 1820.3 ± 107.2 ng/g for groups L, M, and H, respectively. Preliminary experiments revealed that group H significantly inhibited germination indicators in *Ipomoea aquatica*, reducing the germination rate and germination index by approximately 21.3% and 31.2%, respectively. In contrast, group M showed only marginal differences from group L, indicating that a 6-fold increase above background levels did not induce significant phytotoxic effects. Based on these findings, we therefore focused subsequent enzymatic, metabolomic, and transcriptomic analyses on group L and group H, an approach consistent with an earlier study (Yan et al., 2024). Additional experimental details are provided in Text S2.

2.3. Determination of growth indicators

Growth indicators were used to evaluate 6PPD-Q effects on seedling emergence, vigor, and development during seed germination (Text S3). Germination counts were recorded daily at a fixed time. After 7 days of incubation, plants were carefully uprooted and washed with deionized water. After surface moisture was completely dried, fresh weight and plant height were immediately measured in triplicate per treatment group. Then, all samples were frozen in liquid nitrogen and stored at −80 °C. The frozen samples were subsequently lyophilized. Dry weight was measured after the freeze-drying process was complete.

2.4. Sample pretreatment, 6PPD-Q extraction and test methods

The detail information for 6PPD-Q extraction is available in Text S4. Analysis of 6PPD-Q in *Ipomoea aquatica* was analyzed by Ultra-High Performance Liquid Chromatography-Triple Quadrupole Tandem Mass Spectrometry (UPLC-MS/MS; Xevo TQD, Waters Corporation, USA) in positive mode, following previously reported methods (Cao et al.,

2022b; Yu et al., 2024a).

2.5. Measurement of root uptake and translocation factor

To assess 6PPD-Q accumulation in root systems of *Ipomoea aquatica*, root concentration factors (RCFs) were calculated as

$$RCF = \frac{C_r\ [\mathrm{ng/g}]}{C_{soil}\ [\mathrm{ng/g}]} \quad (1)$$

where C_r represented 6PPD-Q concentration in roots and C_{soil} denoted soil concentration.

As interactions of 6PPD-Q with plant roots can influence their translocation into stems and leaves, translocation factors (TFs) were determined as

$$TF_{root-stem} = \frac{C_s\ [\mathrm{ng/g}]}{C_r\ [\mathrm{ng/g}]} \quad (2)$$

$$TF_{root-leaf} = \frac{C_l\ [\mathrm{ng/g}]}{C_r\ [\mathrm{ng/g}]} \quad (3)$$

$$TF_{stem-leaf} = \frac{C_l\ [\mathrm{ng/g}]}{C_s\ [\mathrm{ng/g}]} \quad (4)$$

where C_s, C_l, and C_r corresponded to 6PPD-Q concentrations in stems, leaves, and roots, respectively.

2.6. Determination of enzyme activity

To assess 6PPD-Q effect on the antioxidant system of *Ipomoea aquatica* roots, stems, and leaves, determination of enzyme activity was performed. Details of the determination method are given in Text S5.

2.7. Determination and prediction of toxicity of 6PPD-Q transformation products

To comprehensively evaluate the environmental risk of 6PPD-Q, we identified its major transformation products (TPs) in *Ipomoea aquatica* and predicted their ecotoxicological effects. TPs were characterized using ultra-high performance liquid chromatography coupled with high-resolution Orbitrap mass spectrometry (UPLC-Orbitrap-MS/MS, Thermo Fisher Scientific), and detailed analytical methods are provided in Text S6. We also predicted 6PPD-Q toxicity and its TPs on three trophic levels (green algae, primary producers; Daphnia, primary consumers; fish, secondary consumers) using ECOSAR 2.2. Complete toxicity assessment protocols are available in Text S7.

2.8. Transcriptomics and quantitative real-time PCR analysis

To elucidate 6PPD-Q transformation pathways in *Ipomoea aquatica*, we selected groups L and H for an integrated analysis. Given that roots were recognized as the primary site for both 6PPD-Q uptake and metabolism (Baig et al., 2025; Castan et al., 2023), root tissues were targeted for transcriptomic profiling. Following 7 days of exposure, fresh root samples were collected, thoroughly cleaned, and immediately preserved at −80 °C for subsequent analysis. Detailed protocols are provided for plant RNA extraction, library preparation, and sequencing analysis in Text S8. Transcriptome data reliability was confirmed through quantitative real-time PCR (qRT-PCR) validation, with methodological details described in Text S9.

2.9. Enzyme inhibition experiment

To experimentally verify the role of CYP450s in 6PPD-Q metabolism, we conducted a set of enzyme inhibition experiment. Detailed information can be seen in Text S10.

2.10. Quality control and statistical analysis

To ensure accurate identification and quantification of targeted analytes, comprehensive quality controls were conducted. A solvent blank was analyzed after every 10 samples to monitor instrument contamination and background interference. For quantification of 6PPD-Q, mass-labeled internal standard calibration curves with six points were utilized, demonstrating excellent linearity. Average recoveries of 6PPD-Q in plant tissues were 86.8% ± 6.2% to 104.0% ± 8.7% (Table S1), with relative standard deviations below 15% for the spiked samples (n = 3). Method limits of detection (MLODs) were calculated on the basis of a signal-to-noise ratio of 3. MLODs for 6PPD-Q in *Ipomoea aquatica* were 0.28 ng/g. All treatments were performed in triplicate, and data are presented as mean ± standard deviation (SD) (n = 3). And all 6PPD-Q concentrations are expressed on a dry weight (dw) basis (ng/g dw). Detailed information about statistical analysis is provided in Text S11.

3. Results and discussion

3.1. Uptake, translocation and growth response of 6PPD-Q

6PPD-Q was detected in the roots, stems, and leaves after 7 days of exposure for plants in all treatments, with the highest concentrations consistently observed in roots (Fig. 1A). In group L, accumulation of trace levels of 6PPD-Q (17.8 ± 0.7 ng/g) was consistent with the presence of a moderate amount of 6PPD-Q in the initial soil matrix (33.2 ± 2.1 ng/g). Under medium exposure, *Ipomoea aquatica* roots (55.3 ± 2.9 ng/g) accumulated 1.8-fold higher 6PPD-Q levels than leaves (30.6 ± 1.6 ng/g). In group H, 6PPD-Q root concentration (1414.5 ± 17.3 ng/g) was 10.5-fold higher than that in leaves, consistent with the pattern observed in group M. These findings indicated that 6PPD-Q primarily accumulated in roots across all treatment levels. This behavior can be explained by its high hydrophobicity of 6PPD-Q (log K_{ow} = 5.6), which favors partitioning into root lipids (Castan et al., 2023). The relatively high RCF and low TFs further confirmed this accumulation pattern (Fig. 1B). These results were consistent with the findings reported by Castan et al. (2023), potentially reflecting a general trend for 6PPD-Q behavior in plants. Notably, the relatively high $TF_{stem\text{-}leaf}$ observed in group M likely resulted from enhanced transpiration, which enhanced the apoplastic and xylem translocation of 6PPD-Q to leaves (Kunene and Mahlambi, 2023).

Accumulation dynamics exhibited different profiles across treatments (Fig. 1C). Specifically, group L showed consistent concentrations from Day 3 to 7. Group M and H showed an increasing trend over time with higher absolute values for group H than M. These results indicated that 6PPD-Q accumulation in *Ipomoea aquatica* was not only concentration-dependent but also progressive over time.

Soil physicochemical properties showed no significant differences among groups L, M, and H ($p > 0.05$) (Table S2), indicating that soil conditions did not influence the observed differences in 6PPD-Q uptake. Nevertheless, 6PPD-Q exposure significantly inhibited key germination parameters of *Ipomoea aquatica*, including plant height, fresh weight, dry weight, germination potential, germination rate, germination index, and vigor index ($p < 0.05$, Fig. 1D–F, Fig. S1A–D). In group H, these indices decreased by 12.8%, 22.5%, 16.3%, 26.0%, 21.3%, 31.2%, and 46.6%, respectively, compared with group L. Notably, no significant difference was observed between groups L and M, indicating that inhibitory effects were only evident at the higher exposure concentration. The observed reduction in germination parameters and seedling biomass aligned with the inhibitory effects of 6PPD in wheat reported by Baig et al. (2025), a pattern also seen with tomatoes exposed to high concentrations of tire particles (Wasnik et al., 2026). Overall, these findings underscore a potential dietary exposure risk.

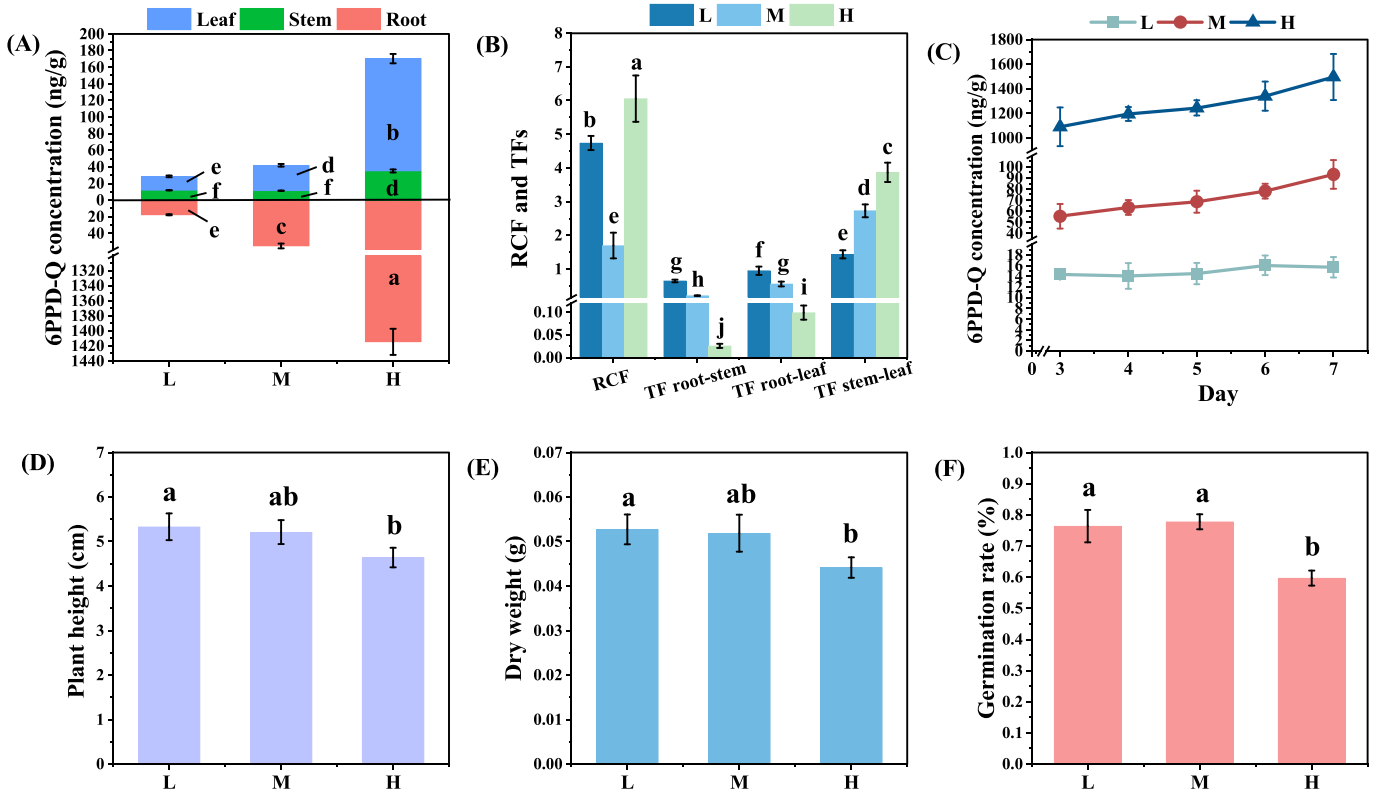

Fig. 1. Uptake, translocation, and growth response of *Ipomoea aquatica* to 6PPD-Q after 7 days of exposure. 6PPD-Q concentration in roots, stems, and leaves under low exposure (L), medium exposure (M) and high exposure (H) conditions (A); Root concentration factor (RCF) and translocation factors (TFs) in group L, M and H (B); Accumulation kinetics of 6PPD-Q in whole plants across groups L, M and H over 7 days exposure period (C); Growth parameters including plant height, dry weight, and germination rate (D-F). Error bars represent the standard deviation values (n = 3). Different letters above bars denote significant differences ($p < 0.05$).

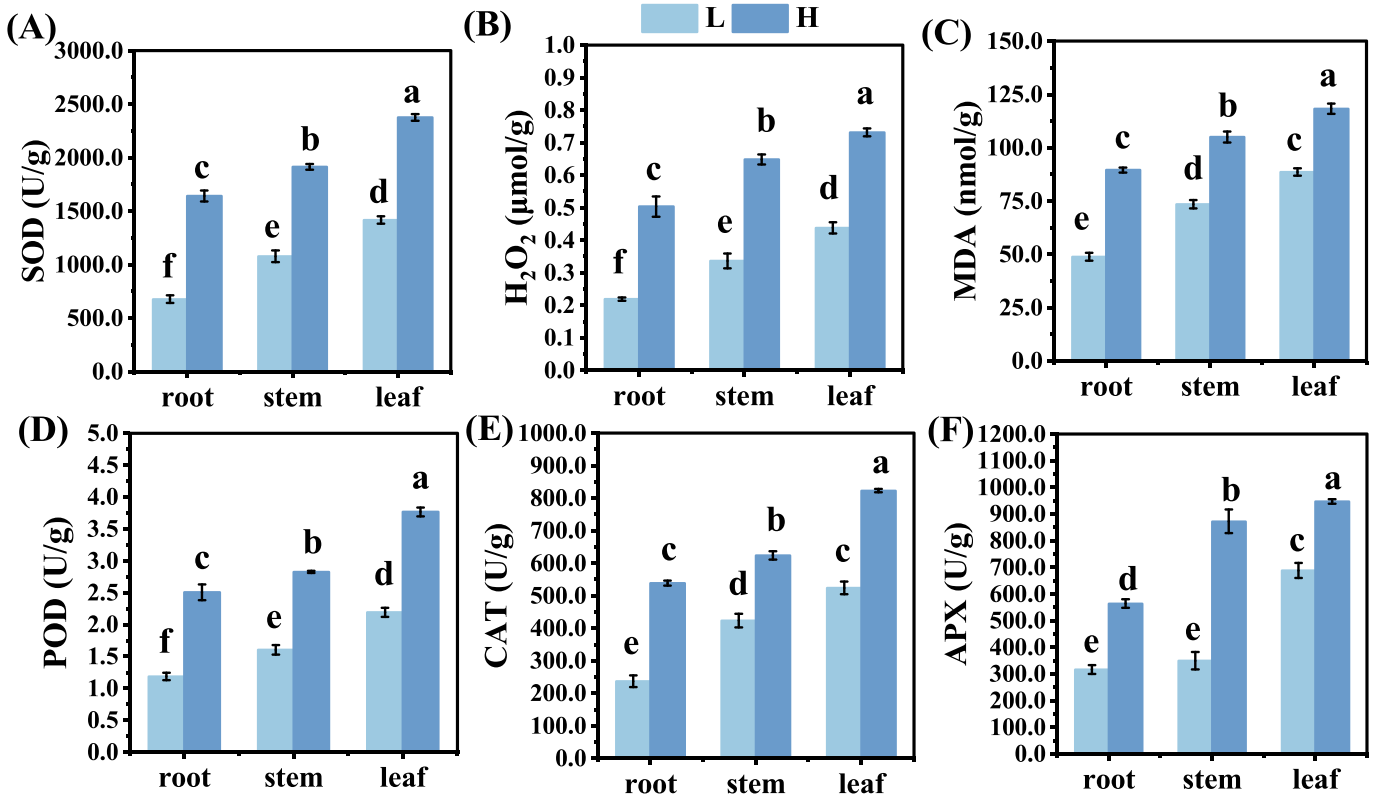

Fig. 2. Effects of 6PPD-Q on enzymatic activities in *Ipomoea aquatica*. (A) SOD; (B) H_2O_2; (C) MDA; (D) POD; (E) CAT; (F) APX. Error bars represent the standard deviation (n = 3). Different lowercase letters above bars denote statistically significant differences ($p < 0.05$).

3.2. Effect of 6PPD-Q on antioxidant enzyme activities in plants

When plants experience oxidative damage, their antioxidant systems are activated to mitigate the adverse effects of external stresses. Fig. 2A–F shows that high exposure to 6PPD-Q significantly enhanced antioxidant enzyme activities in roots, stems, and leaves of germinating *Ipomoea aquatica* compared with group L ($p < 0.05$). Superoxide dismutase (SOD) is the first line of defense against abiotic stress in plants by converting superoxide ($O_2^{-}\bullet$) into hydrogen peroxide (H_2O_2) (Mishra et al., 2023). In group H, SOD activity increased by 1.7- to 2.4-fold compared with group L (Fig. 2A), leading to a 1.7- to 2.3-fold rise in H_2O_2 concentration (Fig. 2B). This accumulated H_2O_2 could be converted into more oxidizing •OH through the Fenton reaction, then attacking cell membranes and causing membrane lipid peroxidation (García-Pérez et al., 2025). The increase of the malondialdehyde (MDA) content in this study also supported this view, which showed a 1.3- to 1.8-fold increase compared with group L (Fig. 2C). Moreover, a 1.7- to 2.1-fold increase in peroxidase (POD) activity helped mitigate this damage by initiating a secondary line of defense (Fig. 2D). Similarly, catalase (CAT) activity also increased by 1.5- to 2.3-fold compared with group L (Fig. 2E) and contributed to H_2O_2 removal, thereby aiding in overcoming tissue metabolic damage (Mhamdi et al., 2010). To mitigate oxidative pressure generated in mitochondria and/or peroxisomes (Eltelib et al., 2012), ascorbate peroxidase (APX) activity increased by 1.4- to 2.5-fold compared with group L (Fig. 2F).

Consistent with findings on MDA accumulation (Bi et al., 2024), leaves exhibited the most pronounced activation of antioxidant enzymes. As the primary site of photosynthesis, leaves are particularly vulnerable to oxidative damage (Patel et al., 2019). We propose that 6PPD-Q exposure may activate NADPH oxidases, leading to an overproduction of H_2O_2 (Wen et al., 2025). This resultant oxidative stress consequently triggers the robust antioxidant defense observed in leaves (Trchounian et al., 2016). In contrast, roots exhibited comparatively weaker antioxidant responses despite their heavier 6PPD-Q accumulation (Fig. 1A). The discrepancy might be explained by two physiological factors. First, the lower metabolic activity and absence of photosynthesis in roots means they had a lower basal production of reactive oxygen species such as H_2O_2 and thus a consequently weaker antioxidant response (Farooq et al., 2019). Furthermore, we hypothesize that roots, as initial stress trigger site, prioritize sending stress signals to the above ground (Mittler et al., 2011). These signals, potentially involving calcium and other electric signals, are transported upward via the vascular system (Gilroy et al., 2016). As the main pathway, stems both carried these signals and reacted to them to a moderate degree. This intermediate level of signal processing likely explained the intermediate antioxidant enzyme activity observed in stems. Overall, these findings provide new insights into how plant tissues differentially cope with oxidative stress induced by emerging pollutants like 6PPD-Q.

3.3. Transformation pathway, relative abundance and toxicity prediction of 6PPD-Q transformation products

A total of 19 TPs of 6PPD-Q were proposed using UPLC-Orbitrap-MS/MS, classified into nine level 3 and ten level 4 intermediates under established confidence levels (Schymanski et al., 2014). Detailed products information and mass spectra are provided in Table S3 and Fig. S2–S3. Based on the putative intermediates, potential metabolic transformation pathways for 6PPD-Q were proposed, involving phase I reactions (hydroxylation, reduction, oxidation, bond cleavage, carboxylation, and elimination) and phase II reactions (glycosylation, methylation, methoxylation, and glutathionylation) (Fig. 3A). Notably, methoxylation, glutathionylation, oxidation, carboxylation, and

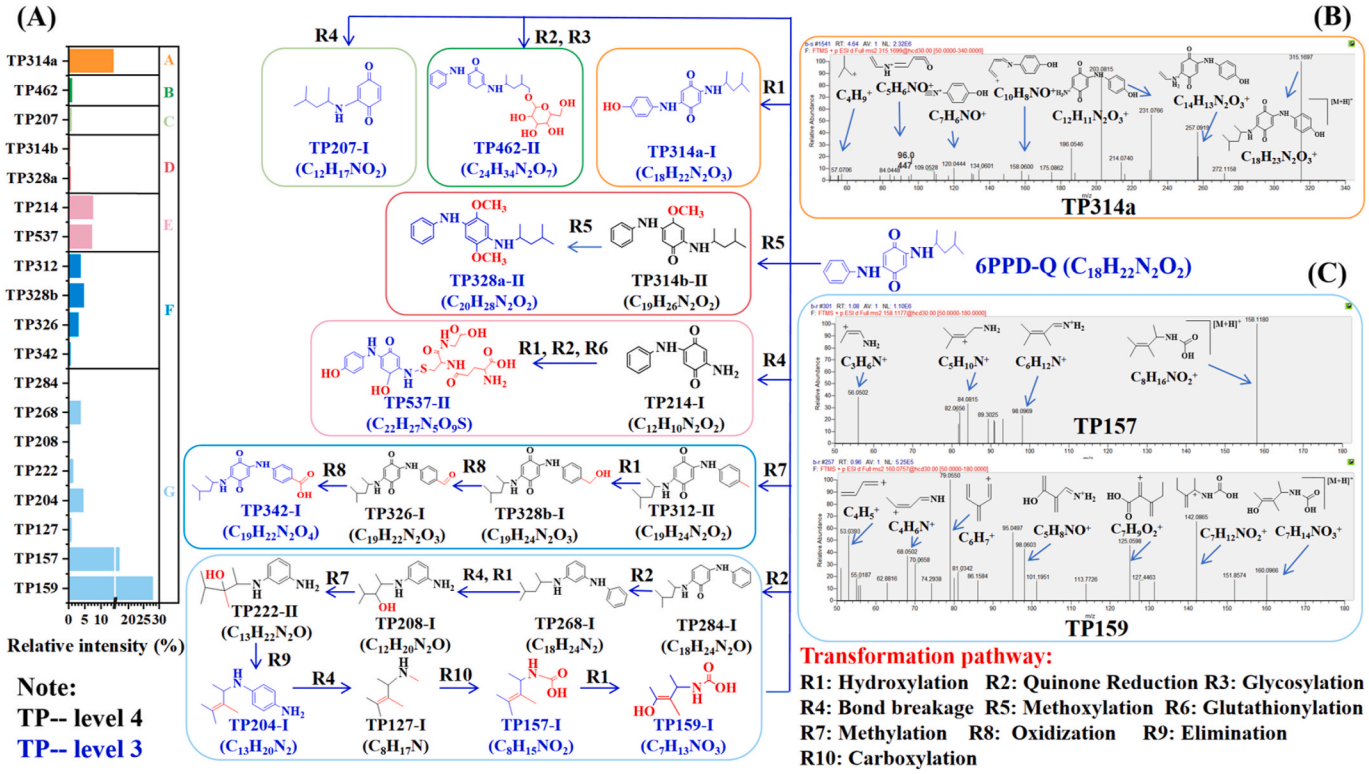

Fig. 3. Metabolic pathways and relative abundance of 6PPD-Q in germinating *Ipomoea aquatica* (A); MS/MS spectra obtained from positive ESI mode of TP314a (B); TP157 and TP159 (C). Compounds labeled with I represent phase I TPs, and compounds labeled with II represent phase II TPs.
Note: Structural elucidation was based on MS fragmentation patterns, and other isomeric forms may exist. Blue marks on the structural formulas represent confidence level 3, and black marks represent confidence level 4. (For interpretation of the references to colour in this figure legend, the reader is referred to the Web version of this article.)

quinone reduction are proposed as putative transformation pathways for 6PPD-Q in plants for the first time. While hydroxylation, glycosylation, methylation, and bond cleavage have been reported in blood (Yang et al., 2024), and elimination in aqueous samples (Yu et al., 2024a), their occurrence in plants is suggested here for the first time. Of the soil-borne 6PPD-Q, 87.3% was taken up by plants and subsequently transformed. To further estimate dominant metabolic routes, the relative abundance of each TP was calculated as its peak area relative to the sum of all such peaks using semi-quantitative analysis (Fig. 3A).

Based on MS/MS fragment spectra and mass relationships among molecules, we tentatively inferred the structures of TPs and proposed metabolic pathways of 6PPD-Q. TP314a (*m/z* 315.1703) was one of the most abundant intermediates, with a relative abundance of 13.7%. It had specific fragments at *m/z* 257.0921 ($[C_{14}H_{13}N_2O_3]^+$), *m/z* 120.0444 ($[C_7H_6NO]^+$), and *m/z* 96.0444 ($[C_5H_6NO]^+$) compared to 6PPD-Q (*m/z* 299.1754) (Fig. 3B). This suggested that the aniline ring of 6PPD-Q could be attacked by •OH, potentially leading to the generation of TP314a by hydroxylation (Yu et al., 2024a). TP207 (*m/z* 208.1332) may represent the loss of an aniline ring from 6PPD-Q, suggesting that cleavage occurred at the quinone moiety. The formation of the carboxylic acid metabolite TP342 (*m/z* 343.1652) was proposed to involve a multi-step pathway. It may have originated from TP312 (*m/z* 313.1911), which appears to possess an additional methyl group at the aniline ring compared to 6PPD-Q. Subsequent •OH attacked on the methyl group could have resulted in its hydroxylation, potentially yielding TP328b (*m/z* 329.1860). The aniline-ring alcohol may then have been oxidized to the aldehyde compound TP326 (*m/z* 327.1703). Finally, this aldehyde compound may have undergone a final oxidation step to form the carboxylic acid TP342. The proposed structure of TP342 was supported by its MS/MS fragments at *m/z* 163.0628 ($[C_9H_9NO_2]^+$) and *m/z* 113.0603 ($[C_6H_9O_2]^+$). Additionally, a novel and multi-step transformation pathway was proposed. First, TP284 (*m/z* 285.1961) may have been formed by the reduction of 6PPD-Q, converting the quinone moiety to a hydroquinone. A subsequent reaction, evidenced by a mass loss of 15.9949 Da, may then have produced TP268 (*m/z* 269.2012). TP208 (*m/z* 209.1648) may have originated from TP268 via mid-chain hydroxylation followed by the terminal C-N bond cleavage, resulting in an aniline group loss. Then, methylation of the mid-chain hydroxyl group may have yielded TP222 (*m/z* 223.1805). Subsequent elimination at the same position may have produced TP204 (*m/z* 205.1699). Following the proposed formation of TP127 (*m/z* 128.1434) from TP204 via anilino group loss, the most abundant transformation products were TP157 (*m/z* 158.1176) and TP159 (*m/z* 160.0968), with relative abundances of 17.2% and 28.0%, respectively (Fig. 3C). TP157, defined by two characteristic fragments at *m/z* 98.0964 ($[C_6H_{12}N]^+$) and *m/z* 84.0808 ($[C_5H_{10}N]^+$), further supported the proposed transformation steps from TP208 to TP204. MS/MS fragments of TP159 at *m/z* 142.0863 ($[C_7H_{12}NO_2]^+$) and *m/z* 98.0600 ($[C_5H_8NO]^+$), suggested a carboxyl group and a terminal hydroxyl, respectively, consistent with the structure with carboxylation at the alpha-carbon. This multi-step pathway, characterized by increasing relative abundance (0.2% to 28.0%) and decreasing molecular mass (*m/z* 285.1961 to *m/z* 160.0968), appears to be the predominant transformation pathway of 6PPD-Q in germinating *Ipomoea aquatica*.

Phase I intermediates may undergo phase II conjugation, potentially yielding glucuronide conjugates, methoxylated metabolites, and GSH conjugates (Yang et al., 2024; Jancova et al., 2010). TP462 (*m/z* 463.2439) formation may have involved quinone reduction to a semiquinone and glucose addition to the branched chain of 6PPD-Q. It also had key fragments at *m/z* 184.1332 ($[C_{10}H_{18}NO_2]^+$) and *m/z* 124.1121 ($[C_8H_{14}N]^+$), suggesting glucosylation at the terminus of the side chain. This was analogous to the glucoside mechanism described by Yu et al. (2024a) in rice and microbiome system, providing further evidence that glucosylation may be a common transformation pathway in plants. In addition, TP314b (*m/z* 315.2067) may have been formed by O-methylation of the quinone moiety in 6PPD-Q, potentially yielding a methoxyquinone. Previous studies have also demonstrated an O-methoxylation pathway for eliminating pentachlorophenol in aquatic plants (Roy and Hänninen, 1994). TP328a (*m/z* 329.2224), which shared most of the fragments with TP314a, may have been further methylated, possibly adding a second methoxy group to form a dimethoxyquinone. Characteristic fragments of TP328a at *m/z* 247.1441 ($[C_{14}H_{19}N_2O_2]^+$) and *m/z* 122.0600 ($[C_7H_8NO]^+$) were consistent with the presence of two methoxy groups on the quinone ring. Furthermore, TP214 (*m/z* 215.0815) had a mass decrease of 84.0939 Da compared to 6PPD-Q (*m/z* 299.1754), suggesting the loss of six methylene (CH_3) groups, with cleavage possibly occurring at the side chain. The GSH conjugation product TP537 (*m/z* 538.1602) may have originated from TP214 and appears to be the dominant phase II intermediates with a relative abundance of 7.2%. TP537 displayed characteristic fragments at *m/z* 301.0614 ($[C_{15}H_{13}N_2O_3S]^+$), *m/z* 149.0379 ($[C_4H_9N_2O_2S]^+$), and *m/z* 91.0542 ($[C_7H_7]^+$). These fragments were consistent with hydroxylation of the benzene ring, quinone reduction, and glutathione conjugation at the amino group. Moreover, TP537 shared the analogous structure resembling 6PPD-Q GSH conjugate reported by Yang et al. (2024), supporting GSH conjugation as a critical phase II metabolic pathway.

Systematic ECOSAR assessment predicted significant ecotoxicological variation among 6PPD-Q and its intermediates (Tables S4–S5). ECOSAR is a predictive tool typically applied to novel chemical structures outside its original training set. The predictions in this study based on ECOSAR primarily focus on aquatic model organisms. Potential risks to higher animals including mammals and humans still require validation through further experiments. Consequently, these results should be interpreted as preliminary estimates of potential toxicity. 6PPD-Q was predicted to have high acute and chronic toxicity to aquatic organisms ($LC_{50}/EC_{50} \leq 1.0$ mg/L and $ChV \leq 0.1$ mg/L). In contrast, the predominant TPs (TP314a, TP157, and TP159) had lower predicted acute and chronic toxicity, due to their relatively lower log K_{ow} values (3.2, 1.4, −0.1, respectively). While these TPs showed lower predicted toxicity, their hydrophilic nature may promote translocation to edible plant parts, thereby increasing potential dietary exposure risk. However, several TPs exhibited elevated predicted toxicity. For instance, TP312 demonstrated higher predicted acute and chronic toxicity than 6PPD-Q, which was attributed to increased lipophilicity form methylation on the benzene ring, thereby enhancing bioaccumulation potential (Abu et al., 2013). Notably, TP284 had 1.3 times higher predicted chronic toxicity to *Daphnia* than 6PPD-Q, potentially due to quinone-hydroquinone redox cycling enhancing oxidative stress (Xu et al., 2021). Furthermore, benzene-ring cleavage products sharing a free amino group (-NH_2) (TP208, TP222, and TP204) also exhibited high predicted *Daphnia* toxicity, with 1.3-, 1.4-, and 1.8-fold greater than 6PPD-Q, indicating the amino group as a key toxicity enhancing factor. Conversely, phase II intermediates like TP462 and TP537 were predicted to be less toxic or harmless ($LC_{50}/EC_{50} > 10$ mg/L and $ChV > 1$ mg/L).

In summary, seven metabolic pathways were proposed for 6PPD-Q in germinating *Ipomoea aquatica*. Among these, hydroxylation played a central role as a key intermediate step, whereas glycosylation, methoxylation, glutathionylation, oxidation, and carboxylation served as the major metabolic pathways. While ECOSAR predictions indicated high theoretical toxicity for some TPs, their actual ecotoxicological effects in planta require validation through *in vivo* bioassays. Furthermore, whether these TPs will translate into a dietary risk via persistent accumulation in edible tissues is a key question for future risk assessment.

3.4. Transcriptional expression and quantitative real-time PCR validation of 6PPD-Q

To elucidate molecular mechanisms underlying 6PPD-Q in *Ipomoea aquatica*, we performed RNA sequencing (RNA-seq). Compared to group L, high exposure of 6PPD-Q induced 1228 differentially expressed genes (DEGs) ($|\log_2\text{Fold Change}| \geq 1$), with 572 up-regulated and 656 down-

regulated (Table S6, Fig. S4). Five randomly selected genes were analyzed by quantitative real-time PCR (qRT-PCR) to verify the transcriptome sequencing results, which were highly consistent with the sequencing data (Fig. 4A). Functional annotation using the Gene Ontology (GO) system revealed that DEGs were significantly enriched in three main categories (Fig. 4B), including cellular components, molecular functions, and biological processes (Tang et al., 2021). Notably, biological processes were predominantly associated with key functions such as transmembrane transport of xenobiotics, activation of functional enzymes, and stress response. Specifically, key enriched GO terms included L-glutamine transmembrane transporter activity, L-glutamate import across plasma membrane, oxidoreductase activity, dioxygenase activity, and lipid storage. We hypothesized that these genes may facilitate the translocation and transformation of 6PPD-Q. Consequently, subsequent analyses focused on genes associated with these critical processes (Tables S7–S9, Fig. 4C).

3.4.1. Transmembrane transport related genes

DEGs related to 6PPD-Q transport are shown in Table S7. Transmembrane transport process is a key step in uptake and internalization of pollutants by plants (Zhang et al., 2025b). Kyoto Encyclopedia of Genes and Genomes (KEGG) pathway annotation results revealed that 6PPD-Q up-regulated a ATP-binding cassette (ABC) transporter gene (*AB2B_ARATH*, 2.4-fold) (Fig. 4D). As the gene is important for organic compound translocation (Wang et al., 2023), the induction likely facilitated 6PPD-Q uptake into root cells. Beyond direct pollutant transport, 6PPD-Q exposure triggered a broader shift in resource metabolism. Genes encoding the lysine histidine transporter (*LHTL8_ARATH*) and amino acid transporter (*AVT1C_ARATH*) were up-regulated by 2.3- and 3.0-fold, respectively, suggesting an enhanced demand for amino acid absorption and recycling under 6PPD-Q stress (Huang et al., 2024; Zhang et al., 2025a). Concurrently, the elevated expression of a sugar transporter gene (*ERDL6_ARATH*, 2.2-fold) indicated a heightened energy demand, which is essential for carbohydrate partitioning and energy balance (Guo et al., 2024).

3.4.2. Transformation related genes

6PPD-Q transformation in *Ipomoea aquatica* was mainly mediated by Phase I (hydroxylation and bond cleavage) and Phase II (glycosylation and glutathionylation) enzymes. Hydroxylation, a key step in aromatic compound oxidation, is facilitated by CYP450s and monooxygenases (Fan et al., 2025). In response to 6PPD-Q exposure, flavonoid and phenylpropanoid metabolic pathways were activated, which was similar to the response observed in *Brassica rapa* L. in previous study (Liu et al., 2025). In our study, the hydroxylated product TP314a was likely generated by the concerted action of up-regulated flavonoid 3′-monooxygenase (*F3PH_PETHY*, 2.7-fold) and CYP450s (*e.g., C7A22_PANGI*, *C78A5_ARATH*, 2.4- to 7.8-fold) (Table S8). The hydroxylated product TP328b was also attributed to CYP450s activity. This was consistent with the established role of these enzymes in oxidizing aromatic structures (Wang et al., 2020). A proposed two-step transformation from 6PPD-Q to the intermediate TP208 (mediated by CYP450s) and then to TP159 was strongly supported by the concurrent induction of a POD (*PER2_ORYSJ*, 2.3-fold). As *PER2_ORYSJ* can activate pollutants and

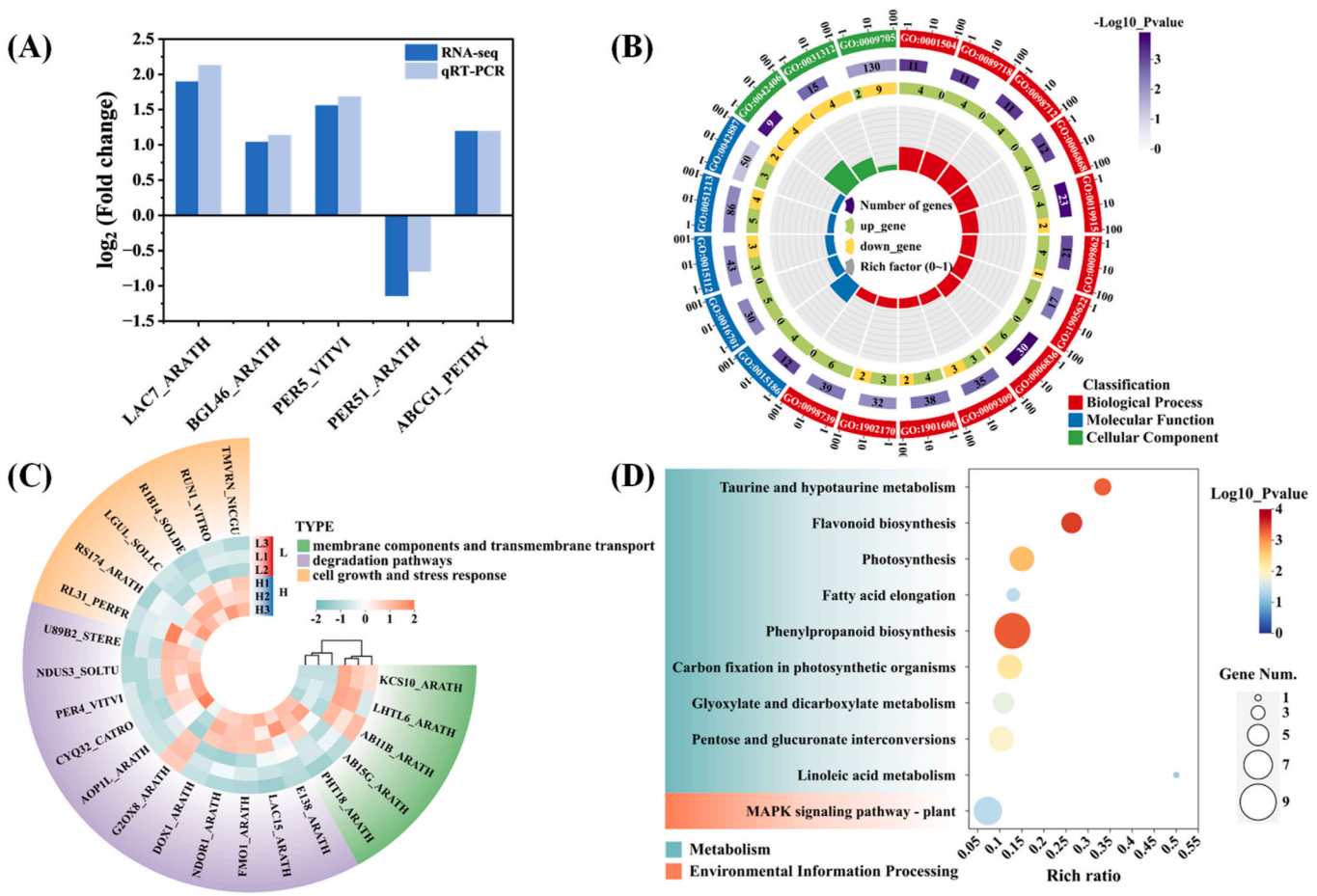

Fig. 4. Transcriptomic analysis of 6PPD-Q in *Ipomoea aquatica*. QRT-PCR validation of DEGs compared with RNA-seq results (A); Gene ontology functional enrichment analysis of differentially expressed genes (DEGs) (B); Clustering heat map of DEGs related to transmembrane transport, biodegradation and stress response (C); Kyoto Encyclopedia of Genes and Genomes pathway functional annotation analysis of DEGs (D).

generate intermediates with hydrophilic functional groups (Wang et al., 2023), we suggest that it may play a role in 6PPD-Q metabolism. This was supported by enzyme inhibitor experiments. Treatment with CYP450 inhibitors caused a dose-dependent increase in 6PPD-Q accumulation (up to 93.5%), and a corresponding decrease in enzyme activity (up to 37.5%), confirming their major role in metabolic clearance (Fig. S5). Phase II conjugation was also prominently activated. The 2.0-fold up-regulated of a glutathione S-Transferase (GST) gene (*GSTUI_ARATH*) likely contributed to the GSH formation conjugated product TP537, thereby reducing 6PPD-Q toxicity (Sousa et al., 2021). Moreover, plant secondary metabolites can be glycosylated by UDP-glycosyltransferase (UGT), which transfers sugar residues from UDP donors to acceptor molecules, forming glycosidic bonds (Louveau and Osbourn, 2019). Glycosylation was implicated by the induction of UGT (*U89B2_STERE*, 2.3-fold) and the detection of corresponding glycosylated metabolites, suggesting a pathway leading to TP462. The marked up-regulation of a UDP-glucose flavonoid 3-O-glucosyltransferase gene (*UFOG7_FRAAN,* 5.7-fold) suggested its potential involvement in this co-metabolic pathway. Collectively, these findings elucidate the molecular mechanisms underpinning the key metabolic pathways of 6PPD-Q in *Ipomoea aquatica*.

3.4.3. *Plant growth and stress response related genes*

Exposure to exogenous pollutants can induce oxidative stress, leading to lipid or protein peroxidation, and DNA damage (Gill and Tuteja, 2010). We identified significant up-regulation of genes encoding key antioxidant enzymes, including *SODC_IPOBA* for SOD, *CATA4_SOYBN* for CAT, and *APX1_PEA* for APX (Table S9). This coordinated up-regulation at the transcriptional level directly explained concomitant increases in enzymatic activities measured in Fig. 2. Transcriptomic analysis also revealed how 6PPD-Q affected the plant's internal structures. The peroxisomal membrane protein gene (*PEX13_ARATH*) was significantly down-regulated by 30%, suggesting possible impairment of peroxisome function (Hu et al., 2012). Such disruption would likely disturb intracellular redox homeostasis. Concurrently, a lipid-transfer protein gene (*DIRL1_ARATH*) was also down-regulated by 50%, which may compromise membrane lipid organization or systemic defense signaling (Maldonado et al., 2002; Salminen et al., 2016). These patterns aligned with the growth-defense tradeoffs (Huot et al., 2014). This indicated that the plant activated its antioxidant defense system while its self-repair capacity was weakened. As a result, energy available for growth was reduced, and fundamental cellular functions were impaired. Therefore, 6PPD-Q likely inhibited seed germination and seedling biomass accumulation by jointly disrupting energy metabolism and membrane integrity. Furthermore, the 2.1-fold up-regulation of a DNA repair protein gene (*XRCC4_ARATH*) indicated the activation of DNA damage repair pathways, potentially in response to the genetic damage induced by oxidative stress (Tang et al., 2021). Simultaneously, ethylene response genes (*e.g., ERF92_ARATH* and *ERF98_ARATH*) in the MAPK signaling pathway were markedly up-regulated (2.0- to 2.7-fold), which

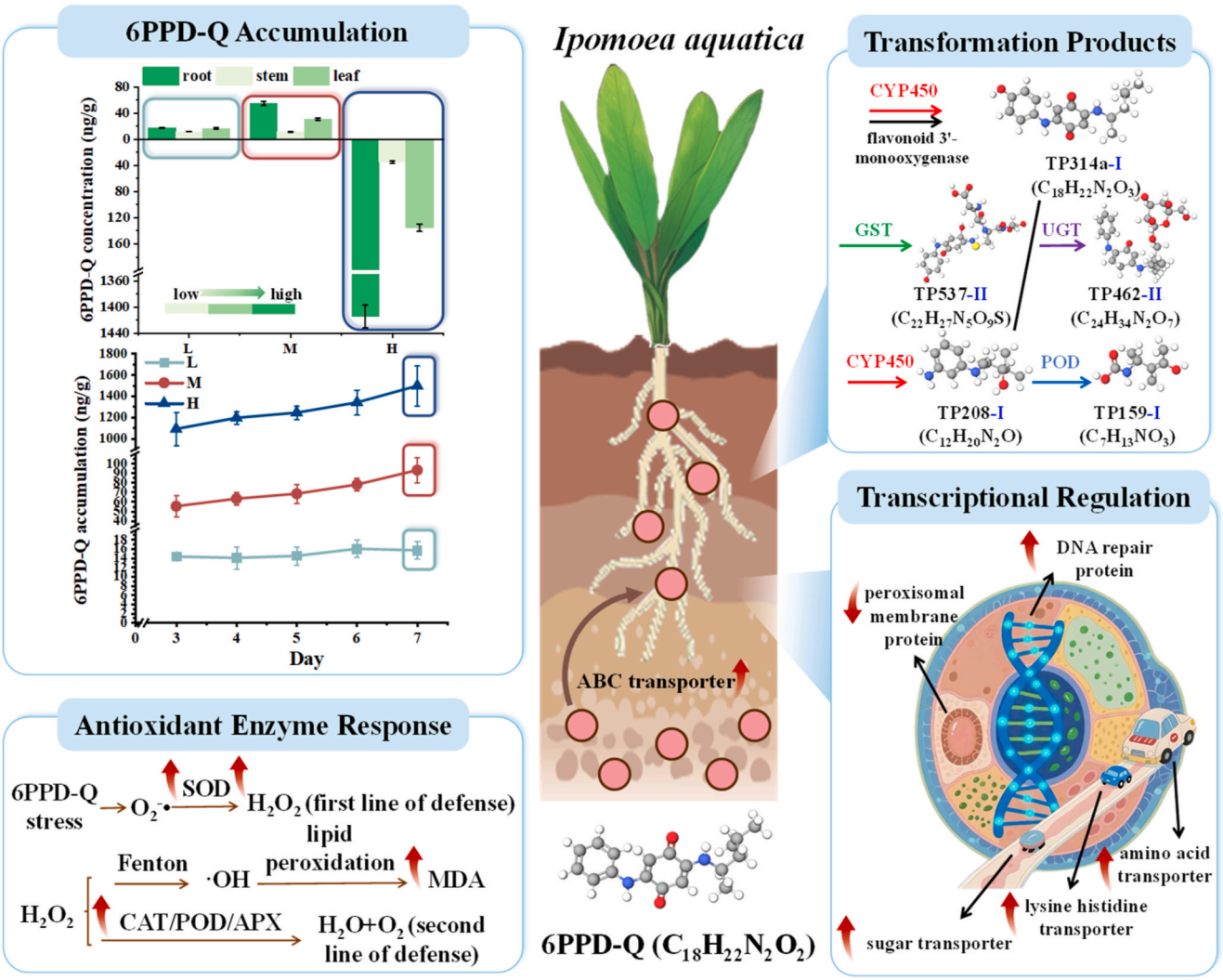

Fig. 5. Conceptual model of 6PPD-Q accumulation, antioxidant response, metabolic transformation, and transcriptional regulation in *Ipomoea aquatica*.

likely amplified stress signaling and reinforced the antioxidant defense system. In summary, 6PPD-Q triggered a chain of internal stresses that compelled the plant to prioritize defense and repair, ultimately leading to growth inhibition.

3.5. Uptake, Transport, and transformation mechanisms of 6PPD-Q

Based on our comprehensive analysis, we propose a model for the environmental fate of 6PPD-Q in *Ipomoea aquatica* (Fig. 5). This model integrates four key aspects, including 6PPD-Q accumulation, antioxidant enzyme response, transformation products, and transcriptomic regulation. 6PPD-Q was taken up by *Ipomoea aquatica* from soil, a process likely facilitated by the up-regulation of ABC transporters in roots. In groups M and H, 6PPD-Q accumulation increased continuously over 7 days. By Day 7, 6PPD-Q predominantly accumulated in roots, reaching 17.8 ± 0.7 ng/g in group L, 55.3 ± 2.9 ng/g in group M, and 1414.5 ± 17.3 ng/g in group H. Under high exposure of 6PPD-Q, the antioxidant enzyme system of *Ipomoea aquatica* was activated. As the conversion of superoxide ($O_2^{\bullet-}$) by SOD produces H_2O_2, we observed the up-regulation of SOD (1.7- to 2.4-fold) and an increase in H_2O_2 concentration (1.7- to 2.3-fold). H_2O_2 likely triggered the Fenton reaction, generating •OH and resulting in lipid peroxidation as indicated by increased MDA (1.3- to 1.8-fold up-regulation) levels. Concurrently, a second defense mechanism was activated, involving CAT (1.5- to 2.3-fold up-regulation), POD (1.7- to 2.1-fold up-regulation), and APX (1.4- to 2.5-fold up-regulation) to scavenge H_2O_2 and converted it into H_2O and O_2. Once inside, 6PPD-Q underwent extensive metabolic transformation. Key phase I reactions included hydroxylation, catalyzed by induced CYP450s and a flavonoid 3′-monooxygenase, yielding TP314a. Subsequent phase II conjugation involved GST and UGT, producing conjugates like TP537 and TP462. A putative two-step pathway was also identified, with CYP450s converting 6PPD-Q to TP208, followed by its subsequent conversion to phase I bond cleavage product TP159 by POD. In addition, 6PPD-Q exposure induced the up-regulation of key genes involved in transmembrane transport (*e.g.,* lysine histidine transporter, amino acid transporter, and sugar transporter), antioxidant and stress responsive genes (*e.g.,* peroxisomal membrane and DNA repair protein).

4. Conclusion

This study provides the first comprehensive insight into 6PPD-Q uptake, translocation, antioxidant response, transformation, and transcriptome responses in germinating *Ipomoea aquatica*. 6PPD-Q preferentially accumulated in roots over aerial tissues in both low, medium and high exposure groups. High exposure of 6PPD-Q significantly inhibited seed germination and seedling growth, which in turn induced oxidative stress. Metabolic analysis revealed that 6PPD-Q underwent extensive Phase I (hydroxylation and bond cleavage) and Phase II (glycosylation and glutathionylation) transformations, mediated by enzymes including CYP450s, POD, GST, and UGT. Several of these pathways (methoxylation, glutathionylation, oxidation, carboxylation, and quinone reduction) were reported here in plants for the first time. Critically, several TPs exhibited higher predicted toxicity than the parent compound, raising concerns about secondary risks. Transcriptomic profiling further revealed the activation of 6PPD-Q transmembrane transport, transformation, and stress response pathways under high 6PPD-Q exposure. However, this analysis was performed only on the low and high exposure groups. Future studies should include multiple exposure concentrations to distinguish dose-dependent responses from general stress. Together, these findings highlight that 6PPD-Q could enter the food chain via consumption of contaminated vegetable and may persist as metabolically stable or even more toxic intermediates. This underscores the need for further research into its environmental fate and potential human exposure risks via dietary intake.

CRediT authorship contribution statement

Shujia Wang: Writing – review & editing, Writing – original draft, Methodology, Investigation, Formal analysis, Data curation, Conceptualization. **Linbin Zhu:** Writing – review & editing, Writing – original draft, Methodology, Investigation, Formal analysis, Data curation, Conceptualization. **Hua Yin:** Writing – review & editing, Writing – original draft, Project administration, Funding acquisition, Conceptualization. **Minghan Zhu:** Writing – review & editing, Software, Resources, Conceptualization. **Yuhao Cai:** Writing – original draft, Software, Methodology, Formal analysis. **Chang He:** Writing – review & editing, Methodology, Investigation, Formal analysis. **Yuanyuan Yu:** Writing – review & editing, Writing – original draft, Project administration, Funding acquisition, Conceptualization. **Shaoyu Tang:** Writing – review & editing, Resources, Methodology, Formal analysis.

Declaration of competing interest

The authors declare that they have no known competing financial interests or personal relationships that could have appeared to influence the work reported in this paper.

Acknowledgments

This study was supported by the National Natural Science Foundation of China of China (42577317, 42307322), the Local Innovation and Entrepreneurship Team Project of Guangdong Special Support Program (2019BT02L218), Guangdong Basic and Applied Basic Research Foundation (2024A1515011651), and the China Postdoctoral Science Foundation (2024M760960).

Appendix A. Supplementary data

Supplementary data to this article can be found online at https://doi.org/10.1016/j.envpol.2026.128111.

Data availability

Data will be made available on request.

References

Abu, N., Akhtar, M.N., Ho, W.Y., Yeap, S.K., Alitheen, N.B., 2013. 3-Bromo-1-hydroxy-9,10-anthraquinone (BHAQ) inhibits growth and migration of the human breast cancer cell lines MCF-7 and MDA-MB231. Molecules 18 (9), 10367–10377. https://doi.org/10.3390/molecules180910367.

Baig, A.M., Liu, W., Zeb, A., Iqbal, H., Khan, S., Shi, R., Tariq, H., Liu, J., Zhao, Y., Li, X., Ge, Y., 2025. Phytotoxic effects of 6PPD on wheat: insights into germination inhibition, oxidative stress, and metabolic disruptions. Environ. Chem. Ecotoxicol. 7, 1158–1168. https://doi.org/10.1016/j.enceco.2025.05.021.

Bauer, A., Luetjohann, J., Hanschen, F.S., Schreiner, M., Kuballa, J., Jantzen, E., Rohn, S., 2018. Identification and characterization of pesticide metabolites in Brassica species by liquid chromatography travelling wave ion mobility quadrupole time-of-flight mass spectrometry (UPLC-TWIMS-QTOF-MS). Food Chem. 244, 292–303. https://doi.org/10.1016/j.foodchem.2017.09.131.

Bi, Y., Tan, H., Zhang, S., Kang, J., 2024. Response mechanism of extracellular polymeric substances synthesized by Alternaria sp. on drought stress in alfalfa (*Medicago sativa* L.). J. Agric. Food Chem. 72 (30), 16812–16824. https://doi.org/10.1021/acs.jafc.4c04009.

Bohara, K., Timilsina, A., Adhikari, K., Kafle, A., Basyal, S., Joshi, P., Yadav, A.K., 2024. A mini review on 6PPD quinone: a new threat to aquaculture and fisheries. Environ. Pollut. 340, 122828. https://doi.org/10.1016/j.envpol.2023.122828.

Boots, B., Russell, C.W., Green, D.S., 2019. Effects of microplastics in soil ecosystems: above and below ground. Environ. Sci. Technol. 53 (19), 11496–11506. https://doi.org/10.1021/acs.est.9b03304.

Cao, G., Wang, W., Zhang, J., Wu, P., Zhao, X., Yang, Z., Hu, D., Cai, Z., 2022a. New evidence of rubber-derived quinones in water, air, and soil. Environ. Sci. Technol. 56 (7), 4142–4150. https://doi.org/10.1021/acs.est.1c07376.

Cao, G., Zhang, J., Wang, W., Wu, P., Ru, Y., Cai, Z., 2022b. Mass spectrometry analysis of a ubiquitous tire rubber-derived quinone in the environment. TrAC Trends Anal. Chem. 157, 116756. https://doi.org/10.1016/j.trac.2022.116756.

Castan, S., Sherman, A., Peng, R., Zumstein, M.T., Wanek, W., Hüffer, T., Hofmann, T., 2023. Uptake, metabolism, and accumulation of tire wear particle-derived

compounds in lettuce. Environ. Sci. Technol. 57 (1), 168–178. https://doi.org/10.1021/acs.est.2c05660.
Deng, B., Yang, K., Zhang, Y., Li, Z., 2016. Can heavy metal pollution defend seed germination against heat stress? Effect of heavy metals (Cu^{2+}, Cd^{2+} and Hg^{2+}) on maize seed germination under high temperature. Environ. Pollut. 216, 41–52. https://doi.org/10.1016/j.envpol.2016.05.050.
Eltelib, H.A., Fujikawa, Y., Esaka, M., 2012. Overexpression of the acerola (*Malpighia glabra*) monodehydroascorbate reductase gene in transgenic tobacco plants results in increased ascorbate levels and enhanced tolerance to salt stress. South Afr. J. Bot. 78, 295–301. https://doi.org/10.1016/j.sajb.2011.08.005.
Fan, J., Liao, Y., Zhao, Y., Wan, J., Wei, Y., Ouyang, Z., 2025. A CYP450 monooxygenase MaCYP82C169 discovered from mulberry leaves catalyzes the methyl oxidation reaction in 1-deoxynojirimycin biosynthesis. Food Biosci. 66, 106177. https://doi.org/10.1016/j.fbio.2025.106177.
Farooq, M.A., Niazi, A.K., Akhtar, J., Saifullah, Farooq, M., Souri, Z., Karimi, N., Rengel, Z., 2019. Acquiring control: the evolution of ROS-induced oxidative stress and redox signaling pathways in plant stress responses. Plant Physiol. Biochem. 141, 353–369. https://doi.org/10.1016/j.plaphy.2019.04.039.
García-Pérez, P., Losada-Barreiro, S., Bravo-Díaz, C., Gallego, P.P., Lucini, L., 2025. Plant oxidative stress and specialized metabolites: a holistic physicochemical and metabolomics perspective. Plant Physiol. Biochem. 227, 110093. https://doi.org/10.1016/j.plaphy.2025.110093.
Gill, S.S., Tuteja, N., 2010. Reactive oxygen species and antioxidant machinery in abiotic stress tolerance in crop plants. Plant Physiol. Biochem. 48 (12), 909–930. https://doi.org/10.1016/j.plaphy.2010.08.016.
Gilroy, S., Białasek, M., Suzuki, N., Górecka, M., Devireddy, A.R., Karpinski, S., Mittler, R., 2016. ROS, calcium, and electric signals: key mediators of rapid systemic signaling in plants. Plant Physiol. 171 (3), 1606–1615. https://doi.org/10.1104/pp.16.00434.
Guo, H., Guan, Z., Liu, Y., Chao, K., Zhu, Q., Zhou, Y., Wu, H., Pi, E., Chen, H., Zeng, H., 2024. Comprehensive identification and expression analyses of sugar transporter genes reveal the role of *GmSTP22* in salt stress resistance in soybean. Plant Physiol. Biochem. 216, 109095. https://doi.org/10.1016/j.plaphy.2024.109095.
He, W., Gu, A., Wang, D., 2023. Four-week repeated exposure to tire derived 6-PPD quinone causes multiple organ injury in male BALB/c mice. Sci. Total Environ. 894, 164842. https://doi.org/10.1016/j.scitotenv.2023.164842.
Hiki, K., Yamamoto, H., 2022. Concentration and leachability of N-(1,3-Dimethylbutyl)-N′-Phenyl-p-Phenylenediamine (6PPD) and its quinone transformation product (6PPD-Q) in road dust collected in Tokyo, Japan. Environ. Pollut. 302, 119082. https://doi.org/10.1016/j.envpol.2022.119082.
Hu, J., Baker, A., Bartel, B., Linka, N., Mullen, R.T., Reumann, S., Zolman, B.K., 2012. Plant peroxisomes: biogenesis and function. Plant Cell 24 (6), 2279–2303. https://doi.org/10.1105/tpc.112.096586.
Hu, X., Zhao, H., Tian, Z., Peter, K.T., Dodd, M.C., Kolodziej, E.P., 2022. Transformation product formation upon heterogeneous ozonation of the tire rubber antioxidant 6PPD (N-(1,3-dimethylbutyl)-N′-phenyl-p-phenylenediamine). Environ. Sci. Technol. Lett. 9 (5), 413–419. https://doi.org/10.1021/acs.estlett.2c00187.
Hua, X., Feng, X., Liang, G., Chao, J., Wang, D., 2023. Exposure to 6-PPD quinone at environmentally relevant concentrations causes abnormal locomotion behaviors and neurodegeneration in caenorhabditis elegans. Environ. Sci. Technol. 57 (12), 4940–4950. https://doi.org/10.1021/acs.est.2c08644.
Huang, W., Ma, D., Zaman, F., Hao, X., Xia, L., Zhang, E., Wang, P., Wang, M., Guo, F., Wang, Y., Ni, D., Zhao, H., 2024. Identification of the lysine and histidine transporter family in Camellia sinensis and the characterizations in nitrogen utilization. Hortic. Plant J. 10 (1), 273–287. https://doi.org/10.1016/j.hpj.2023.01.009.
Huot, B., Yao, J., Montgomery, B.L., He, S., 2014. Growth-defense tradeoffs in plants: a balancing act to optimize fitness. Mol. Plant 7 (8), 1267–1287. https://doi.org/10.1093/mp/ssu049.
Jancova, P., Anzenbacher, P., Anzenbacherova, E., 2010. Phase II drug metabolizing enzymes. Biomed Pap. 154 (2), 103–116. https://doi.org/10.5507/bp.2010.017.
Kunene, P.N., Mahlambi, P.N., 2023. Case study on antiretroviral drugs uptake from soil irrigated with contaminated water: Bio-accumulation and bio-translocation to roots, stem, leaves, and fruits. Environ. Pollut. 319, 121004. https://doi.org/10.1016/j.envpol.2023.121004.
Kurade, M.B., Xiong, J., Govindwar, S.P., Roh, H., Saratale, G.D., Jeon, B., Lim, H., 2019. Uptake and biodegradation of emerging contaminant sulfamethoxazole from aqueous phase using *Ipomoea aquatica*. Chemosphere 225, 696–704. https://doi.org/10.1016/j.chemosphere.2019.03.086.
Liu, J., Liu, W., Shi, R., Yu, M., Li, X., Ge, Y., Wang, X., Sun, Y., 2025. Pakchoi (*Brassica rapa* L.) modulates the antioxidant system and energy metabolism in response to 6PPD and 6PPD-Q. J. Agric. Food Chem. 73 (31), 19753–19763. https://doi.org/10.1021/acs.jafc.5c04123.
Liu, Z., Feng, Y., Sun, W., Wang, B., Shi, C., Ran, R., Zhang, Y., Lu, L., Zhang, H., 2024. Environmental concentrations of 6PPD and 6PPD-quinone induce hepatic lipid metabolism disorders in male black-spotted frogs. J. Hazard. Mater. 480, 136400. https://doi.org/10.1016/j.jhazmat.2024.136400.
Louveau, T., Osbourn, A., 2019. The sweet side of plant-specialized metabolism. CSH. Perspect Biol. 11, a034744. https://doi.org/10.1101/cshperspect.a034744.
Maldonado, A.M., Doerner, P., Dixon, R.A., Lamb, C.J., Cameron, R.K., 2002. A putative lipid transfer protein involved in systemic resistance signalling in *Arabidopsis*. Nature 419 (6905), 399–403. https://doi.org/10.1038/nature00962.
Mhamdi, A., Queval, G., Chaouch, S., Vanderauwera, S., Van Breusegem, F., Noctor, G., 2010. Catalase function in plants: a focus on arabidopsis mutants as stress-mimic models. J. Exp. Bot. 61 (15), 4197–4220. https://doi.org/10.1093/jxb/erq282.
Mishra, N., Jiang, C., Chen, L., Paul, A., Chatterjee, A., Shen, G., 2023. Achieving abiotic stress tolerance in plants through antioxidative defense mechanisms. Front. Plant Sci. 14, 1110622. https://doi.org/10.3389/fpls.2023.1110622.
Mittler, R., Vanderauwera, S., Suzuki, N., Miller, G., Tognetti, V.B., Vandepoele, K., Gollery, M., Shulaev, V., Van Breusegem, F., 2011. ROS signaling: the new wave? Trends Plant Sci. 16 (6), 300–309. https://doi.org/10.1016/j.tplants.2011.03.007.
Patel, M.K., Pandey, S., Burritt, D.J., Tran, P.L., 2019. Plant responses to low-oxygen stress: interplay between ROS and NO signaling pathways. Environ. Exp. Bot. 161, 134–142. https://doi.org/10.1016/j.envexpbot.2019.02.013.
Rossomme, E., Hart-Cooper, W.M., Orts, W.J., McMahan, C.M., Head-Gordon, M., 2023. Computational studies of rubber ozonation explain the effectiveness of 6PPD as an antidegradant and the mechanism of its quinone formation. Environ. Sci. Technol. 57 (13), 5216–5230. https://doi.org/10.1021/acs.est.2c08717.
Roy, S., Hänninen, O., 1994. Pentachlorophenol: uptake/elimination kinetics and metabolism in an aquatic plant, *Eichhornia Crassipes*. Environ. Toxicol. Chem. 13 (5), 763–773. https://doi.org/10.1002/etc.5620130511.
Salminen, T.A., Blomqvist, K., Edqvist, J., 2016. Lipid transfer proteins: classification, nomenclature, structure, and function. Planta 244 (5), 971–997. https://doi.org/10.1007/s00425-016-2585-4.
Schymanski, E.L., Jeon, J., Gulde, R., Fenner, K., Ruff, M., Singer, H.P., Hollender, J., 2014. Identifying small molecules via high resolution mass spectrometry: communicating confidence. Environ. Sci. Technol. 48 (4), 2097–2098. https://doi.org/10.1021/es5002105.
Seneviratne, M., Rajakaruna, N., Rizwan, M., Madawala, H., Ok, Y.S., Vithanage, M., 2019. Heavy metal-induced oxidative stress on seed germination and seedling development: a critical review. Environ. Geochem. Health 41 (4), 1813–1831. https://doi.org/10.1007/s10653-017-0005-8.
Shi, C., Wu, F., Zhao, Z., Ye, T., Luo, X., Wu, Y., Liu, Z., Zhang, H., 2024. Effects of environmental concentrations of 6PPD and its quinone metabolite on the growth and reproduction of freshwater cladoceran. Sci. Total Environ. 948, 175018. https://doi.org/10.1016/j.scitotenv.2024.175018.
Shi, R., Liu, W., Lian, Y., Wang, Q., Zeb, A., Tang, J., 2022. Phytotoxicity of polystyrene, polyethylene and polypropylene microplastics on tomato (*Lycopersicon esculentum* L.). J. Environ. Manag. 317, 115441. https://doi.org/10.1016/j.jenvman.2022.115441.
Sousa, B., Lopes, J., Leal, A., Martins, M., Soares, C., Azenha, M., Fidalgo, F., Teixeira, J., 2021. Specific glutathione-S-transferases ensure an efficient detoxification of diclofenac in *Solanum lycopersicum*. L. plants. Plant Physiol. Biochem. 168, 263–271. https://doi.org/10.1016/j.plaphy.2021.10.019.
Sun, J., Chen, Q., Qian, Z., Zheng, Y., Yu, S., Zhang, A., 2018. Plant uptake and metabolism of 2,4-Dibromophenol in carrot: in vitro enzymatic direct conjugation. J. Agric. Food Chem. 66 (17), 4328–4335. https://doi.org/10.1021/acs.jafc.8b00543.
Sun, W., Wang, B., Zhang, S., Liu, Z., Zhang, Y., Zhang, H., 2025. Transcriptomic and proteomic insights into 6PPD/6PPD-Q induced oxidative stress in black-spotted frogs. Antioxidants 14 (8), 1019. https://doi.org/10.3390/antiox14081019.
Tang, S., Yin, H., Yu, X., Chen, S., Lu, G., Dang, Z., 2021. Transcriptome profiling of Pseudomonas aeruginosa YH reveals mechanisms of 2, 2′, 4, 4′-tetrabrominated diphenyl ether tolerance and biotransformation. J. Hazard. Mater. 403, 124038. https://doi.org/10.1016/j.jhazmat.2020.124038.
Tanoue, R., Sato, Y., Motoyama, M., Nakagawa, S., Shinohara, R., Nomiyama, K., 2012. Plant uptake of pharmaceutical chemicals detected in recycled organic manure and reclaimed wastewater. J. Agric. Food Chem. 60 (41), 10203–10211. https://doi.org/10.1021/jf303142t.
Tian, Z., Gonzalez, M., Rideout, C.A., Zhao, H., Hu, X., Wetzel, J., Mudrock, E., James, C. A., McIntyre, J.K., Kolodziej, E.P., 2022. 6PPD-Quinone: revised toxicity assessment and quantification with a commercial standard. Environ. Sci. Technol. Lett. 9 (2), 140–146. https://doi.org/10.1021/acs.estlett.1c00910.
Tian, Z., Zhao, H., Peter, K.T., Gonzalez, M., Wetzel, J., Wu, C., Hu, X., Prat, J., Mudrock, E., Hettinger, R., et al., 2021. A ubiquitous tire rubber–derived chemical induces acute mortality in coho salmon. Science 371 (6525), 185–189. https://doi.org/10.1126/science.abd6951.
Trchounian, A., Petrosyan, M., Sahakyan, N., 2016. Plant cell redox homeostasis and reactive oxygen species. In: Gupta, D., Palma, J., Corpas, F. (Eds.), Redox State as a Central Regulator of plant-cell Stress Responses. Springer, Cham, pp. 25–50. https://doi.org/10.1007/978-3-319-44081-1_2.
Wang, B., Sun, W., Ye, X., Liu, Z., Zhang, H., 2025a. Occurrence, analytical methods, and ecotoxicological effects of 6PPD-Quinone in aquatic environments: a review. Trends Anal. Chem. 193, 118449. https://doi.org/10.1016/j.trac.2025.118449.
Wang, G., Wang, X., Liu, Y., Liu, S., Xing, Z., Guo, P., Li, C., Wang, H., 2023. Novel insights into uptake, translocation, and transformation mechanisms of 2,2′,4,4′-tetra brominated diphenyl ether (BDE-47) in wheat (*Triticum aestivum* L.): implication by compound-specific stable isotope and transcriptome analysis. Environ. Sci. Technol. 57 (40), 15266–15276. https://doi.org/10.1021/acs.est.3c04898.
Wang, W., Huang, G., Miao, F., Zhao, Z., Cai, Z., 2025b. Biotransformation of tire-derived 6PPD and 6PPD-Q in soil nematode *Caenorhabditis elegans*: unraveling novel phosphorylation products and distinct kinetic profiles. Environ. Sci. Technol. 59 (28), 14625–14636. https://doi.org/10.1021/acs.est.5c02072.
Wang, W., Wang, J., Wu, Y., Li, D., Allan, A., Yin, X., 2020. Genome-wide analysis of coding and non-coding RNA reveals a conserved miR164-NAC regulatory pathway for fruit ripening. New Phytol. 225 (4), 1618–1634. https://doi.org/10.1111/nph.16233.
Wasnik, S., Cheng, S., Keang, K., Zhang, H., Cross, J.S., 2026. Impact of tire particles and tire leachate contaminants on plant physiology and soil health: case study in mung bean and tomato. NanoImpact 41, 100601. https://doi.org/10.1016/j.impact.2025.100601.

Wen, Y., Zhou, Y., Ding, M., Luo, Z., Wang, C., Pan, Y., He, Y., Jiang, D., 2025. *OsGSTT3* regulates seed germination by modulating reactive oxygen species homeostasis in rice. Theor. Appl. Genet. 138, 302. https://doi.org/10.1007/s00122-025-05092-7.

Xia, B., Wang, S., Li, R., Dong, F., Zheng, Y., Li, Y., 2024. From water to water: insight into the translocation of pesticides from plant rhizosphere solution to leaf guttation and the associated ecological risks. Environ. Sci. Technol. 58 (17), 7600–7608. https://doi.org/10.1021/acs.est.3c10925.

Xu, L., Wang, Y., Song, E., Song, Y., 2021. Nucleophilic and redox properties of polybrominated diphenyl ether derived-quinone/hydroquinone metabolites are responsible for their neurotoxicity. J. Hazard. Mater. 420, 126697. https://doi.org/10.1016/j.jhazmat.2021.126697.

Yan, J., Fang, L., Ni, A., Xi, M., Li, J., Zhou, X., Qian, Q., Wang, Z., Wang, X., Wang, H., 2024. Long-Term neurotoxic effects and Alzheimer's disease risk of early EHDPP exposure in zebrafish: insights from molecular mechanisms to adult pathology. Environ. Sci. Technol. 58 (43), 19152–19164. https://doi.org/10.1021/acs.est.4c05793.

Yang, Y., Meng, W., Zhang, Y., Meng, W., Li, J., Liu, W., Su, G., 2024. Characterizing the metabolism of tire rubber-derived p-phenylenediamine quinones to identify potential exposure biomarkers in humans. Environ. Sci. Technol. 58 (41), 18098–18108. https://doi.org/10.1021/acs.est.4c04693.

Yu, W., Tang, S., Wong, J., Luo, Z., Li, Z., Thai, P., Zhu, M., Yin, H., Niu, J., 2024a. Degradation and detoxification of 6PPD-quinone in water by ultraviolet-activated peroxymonosulfate: mechanisms, byproducts, and impact on sediment microbial community. Water Res. 263, 122210. https://doi.org/10.1016/j.watres.2024.122210.

Yu, Y., Ai, T., Huang, J., Jin, L., Yu, X., Zhu, X., Sun, J., Zhu, L., 2024b. Metabolism of isodecyl diphenyl phosphate in rice and microbiome system: differential metabolic pathways and underlying mechanisms. Environ. Pollut. 361, 124803. https://doi.org/10.1016/j.envpol.2024.124803.

Zhang, C., Shi, M., Lin, Y., Chen, Q., Shi, X., 2025a. Effects of two amino acid transporter-like genes on potato growth. J. Plant Physiol. 304, 154408. https://doi.org/10.1016/j.jplph.2024.154408.

Zhang, J., Zhu, M., Ouyang, X., Yuan, Y., Tang, S., Yin, H., 2025b. Co-metabolism degradation of tetrabromobisphenol A by the newly isolated *Sphingobium sp.* strain QY1-1: multiple metabolic pathways, toxicity evaluation, and mechanisms. J. Hazard. Mater. 488, 137440. https://doi.org/10.1016/j.jhazmat.2025.137440.

Zhang, Z., Dai, C., Chen, S., Hu, H., Kang, R., Xu, X., Huo, X., 2024. Spatiotemporal variation of 6PPD and 6PPDQ in dust and soil from e-waste recycling areas. Sci. Total Environ. 923, 171495. https://doi.org/10.1016/j.scitotenv.2024.171495.